Electron acceleration due to inertial Alfvén waves in a non-Maxwellian plasma

C. E. J. Watt[1] and R. Rankin[1]

Received 9 June 2006; revised 29 November 2006; accepted 14 December 2006; published 28 April 2007.

[1] We investigate parallel electron acceleration due to inertial Alfvén wave pulses in the presence of Lorentzian (kappa) distribution functions which possess high-energy tails. A linear kinetic dispersion relation for inertial Alfvén waves is derived whose solutions are used to guide the analysis of the simulation results. The dispersion relation solutions show that the parallel phase velocity of linear waves is unchanged when Lorentzian distribution functions are considered instead of Maxwellian distribution functions. The solutions also indicate that Landau damping is increased for low values of spectral index, κ, implying that wave-particle interactions are enhanced for Lorentzian distribution functions. We test this hypothesis by performing self-consistent kinetic simulations and show that the energy content of resonant beam electrons significantly increases with decreasing κ. The dependence of this process on pulse amplitude and perpendicular scale length is investigated, and it is shown that for the same pulse parameters, resonant electron beams are generated more efficiently in a Lorentzian plasma compared to a Maxwellian plasma. The energy range of resonant beam electrons are also presented, and it is noted that for low values of κ it is possible to generate electrons with energy of a few keV, even for relatively small-amplitude pulses with peak perpendicular electric fields of the order of 20 mV/m. We also show that the percentage of wave Poynting flux which is converted into electron energy flux depends upon the value of κ, the perpendicular scale length, and the initial amplitude of the inertial Alfvén wave.

Citation: Watt, C. E. J., and R. Rankin (2007), Electron acceleration due to inertial Alfvén waves in a non-Maxwellian plasma, *J. Geophys. Res.*, *112*, A04214, doi:10.1029/2006JA011907.

1. Introduction

[2] An abundance of in situ rocket and satellite observations indicate that time-varying signatures of high-energy (100 eV to 10 keV) electrons are associated with Alfvénic electromagnetic waves [*Boehm et al.*, 1990; *Ivchenko et al.*, 1999; *Chaston et al.*, 2000, 2002, 2003, 2005; *Khoyaintsev et al.*, 2000; *Andersson et al.*, 2002; *Su et al.*, 2004; *Ergun et al.*, 2005]. This has inspired a considerable modeling effort focussed upon the interaction between electrons and shear Alfvén waves along geomagnetic field lines in order to better understand the time-varying acceleration processes which may be active above auroral regions. Shear Alfvén waves generate nonnegligible parallel electric fields when their perpendicular scale length is short, comparable to the ion acoustic gyroradius $\rho_{ia} = C_s/\Omega_i$ [*Hasegawa*, 1976] or electron skin depth $\lambda_e = c/\omega_{pe}$ [*Goertz and Boswell*, 1979]. Here, $C_s = (2k_bT_e/m_i)^{1/2}$ is the ion acoustic speed, $\Omega_i = q_iB_0/m_i$ is the ion gyrofrequency, $\omega_{pe} = (n_eq_e^2/(m_e\varepsilon_0))^{1/2}$ is the electron plasma frequency, and n_α is the number density, T_α is the temperature, m_α is the mass, and q_α is the charge of plasma species α. On the whole, modeling studies have focused on the inertial regime $k_\perp\lambda_e \sim 1$, since this regime is more appropriate for altitudes less than $4-5R_E$ [*Lysak and Carlson*, 1981], where evidence suggests the auroral acceleration region is located.

[3] Various approaches can be used to study Alfvénic acceleration. *Kletzing* [1994] used a Liouville mapping in phase-space to demonstrate how Alfvénic disturbances with small perpendicular scales can accelerate electrons up to keV energies. More recently, this approach has been used to investigate the resonant acceleration (and deceleration) of electrons by shear Alfvén waves in the presence of a high-energy inverted-V population [*Chen et al.*, 2005]. In test-particle simulations, *Thompson and Lysak* [1996] showed that they could reproduce some of the specific features of electron conic signatures associated with electron acceleration, although a static potential drop was required in addition to the wave accelerating potential. Test-particle approaches have continued to provide much insight into acceleration processes [e.g., *Chaston et al.*, 2002], including the investigation of the consequences of including both kinetic ($k_\perp\rho_{ia} \sim 1$) and inertial ($k_\perp\lambda_e \sim 1$) effects on the parallel electric field generated by the wave [*Chaston et al.*, 2003], as well as a study of the effect of including different plasma density profiles along the field line [*Su et al.*, 2004]. There have also been self-consistent hybrid simulation studies into the interaction between small-scale Alfvén waves and the surrounding plasma. These have shown that

[1]Department of Physics, University of Alberta, Edmonton, Alberta, Canada.

0148-0227/07/2006JA011907

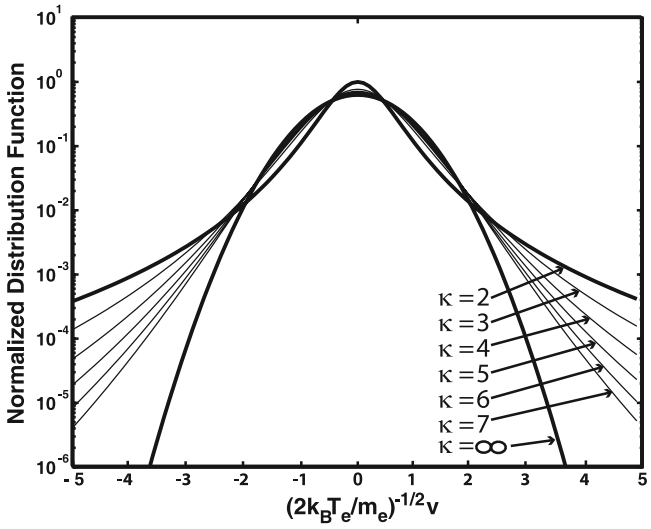

Figure 1. Lorentzian and Maxwellian nondrifting distribution functions for equal number density and temperature. Varying κ values indicated in the figure.

the nonlinear steepening of waves, and electron trapping in the wave, are important parts of the acceleration process [*Hui and Seyler*, 1992, *Seyler et al.*, 1995, *Clark and Seyler*, 1999].

[4] Using a self-consistent Vlasov-kinetic model, *Watt et al.* [2004, 2005, 2006] have shown that nonlinear wave-plasma interactions are important for resonant electron acceleration in inertial Alfvén waves. Their simulation results demonstrated that the energy and number of accelerated electrons depends sensitively on both the amplitude of the Alfvén disturbance and the perpendicular scale length of the Alfvén disturbance. It was shown that the electrons could extract up to 20% of the wave Poynting flux during the acceleration process. The effect of including the mirror force was also investigated [*Watt et al.*, 2006], where it was shown that electrons can be accelerated at more than one location along the magnetic field line. As Alfvén waves move down geomagnetic field lines, into regions of higher Alfvén speed, they catch up with previously accelerated electrons and accelerate them again. It is important to investigate factors which may modify the basic acceleration process. To this end, we have performed simulation studies where we focus on a parameter that has not yet been studied in the context of inertial Alfvén wave acceleration: the form of the ambient electron distribution function that is the source of resonantly accelerated electrons.

[5] Electron distribution functions in the auroral source region and along geomagnetic field lines above the auroral oval are often observed with high-energy tails that can be modeled by a Lorentzian (kappa) distribution with $\kappa < 7$ [*Christon et al.*, 1988; *Olsson and Janhunen*, 1998; *Kletzing et al.*, 2003]. The study of field-aligned electron acceleration along geomagnetic field lines should therefore be performed in the presence of such plasma.

[6] The aim of this paper is to investigate the efficiency of parallel electron acceleration due to inertial Alfvén wave (IAW) pulses (i.e., Alfvénic disturbances with perpendicular scales $\lambda_\perp$ similar to the electron skin depth λ_e) for both Lorentzian and Maxwellian electron distribution functions. A kinetic dispersion relation for inertial Alfvén waves is derived for Lorentzian distribution functions and presented in section 2. Section 3 contains a description of the kinetic simulation model which is used to obtain the results presented in this paper. The model is used to investigate the total energy content of resonant electron beam (section 4), the energy range of resonant beam electrons (section 5), and the percentage conversion of wave Poynting flux to electron energy flux (section 6). The simulation results are discussed in section 7 and the conclusions of this paper are presented in section 8.

2. Kinetic Dispersion Relation

[7] Resonant electron acceleration in inertial Alfvén waves depends sensitively on the phase velocity of the wave, which exhibits a strong dependence on perpendicular wave number [*Lysak and Lotko*, 1996]. If the perpendicular scale is decreased to the electron skin depth, the phase velocity is correspondingly reduced to a fraction of the local Alfvén speed, allowing more interaction between the wave and the thermal plasma. *Watt and Rankin* [2007] show that the phase velocity of propagating inertial Alfvén wave pulses in full Vlasov kinetic simulations agrees well with solutions of the linear dispersion relation. This was unexpected, since the simulation model is nonlinear and includes the full interaction between the wave and the electron distribution function, f_e. In particular, a strong perturbation of f_e is needed to carry the wave parallel current when the amplitude of the waves is large. However, in simulations involving large-amplitude waves, it was found that phase velocities are still well approximated by the linear dispersion relation. It is instructive therefore to investigate whether this is the case when a Lorentzian form of the electron distribution function is used. We use the linear dispersion relation solutions as an aid to the interpretation of the simulation results documented in this paper.

[8] The standard distribution function considered for kinetic plasma effects is the Maxwellian distribution function (given here in its one-dimensional form):

$$f_e(v) = \left(\frac{n_e}{\alpha_{e,M}\sqrt{\pi}}\right) \exp\left[-\left(\frac{v^2}{\alpha_{e,M}^2}\right)\right], \tag{1}$$

where $\alpha_{e,M} = (2k_BT_e/m_e)^{1/2}$ is the thermal speed of the Maxwellian plasma. The Lorentzian, or kappa, distribution function, is defined here in its one-dimensional form [*Summers and Thorne*, 1991],

$$f_e(v) = \left(\frac{n}{\theta_e\sqrt{\pi}}\right) \frac{\Gamma(\kappa+1)}{\kappa^{3/2}\Gamma(\kappa-1/2)} \left(1+\frac{v^2}{\kappa\theta_e^2}\right)^{-\kappa}, \tag{2}$$

where $\theta_e = [(2\kappa - 3)/\kappa]^{1/2}$ $(k_bT_e/m_e)^{1/2}$ and Γ is the usual gamma function [*Abramowitz and Stegun*, 1972]. We will assume in this paper that $\kappa \geq 2$ and $\kappa \in \mathbf{Z}$. The observations mentioned in the introduction suggest that κ can have noninteger values, but we use integer values here in order to keep the mathematical analysis simple. If we take the limit of equation (2) as $\kappa \to \infty$, then we recover the Maxwellian distribution function in equation (1).

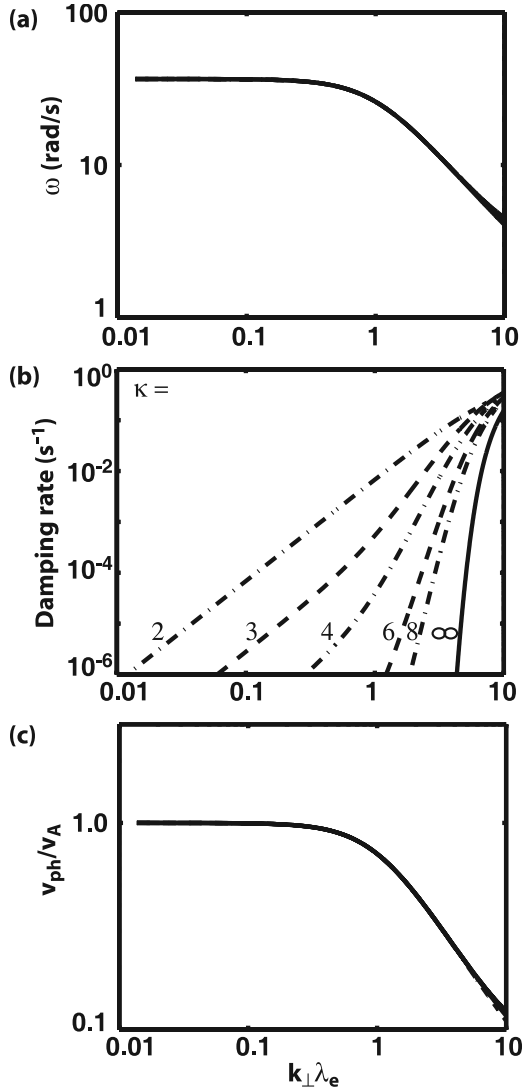

Figure 2. Solutions of the kinetic dispersion relation for Lorentzian distribution functions: (a) real part of frequency, (b) damping rate, and (c) parallel phase velocity for varying perpendicular wave number.

[9] Figure 1 shows the dependence of the one-dimensional electron distribution function on different values of κ ($\kappa = \infty$ corresponds to a Maxwellian distribution function). Each distribution function shown in this figure has the same number density and temperature, as well as zero electron drift. The high-energy tail of the Lorentzian is clearly visible for all values of $\kappa \leq 7$, whereas the Maxwellian form drops off more steeply at high velocities.

[10] We have derived a kinetic dispersion relation for inertial Alfvén waves in Lorentzian plasma assuming that the ions are cold and do not contribute to plasma dynamics in the field-aligned direction. This is valid for investigating the plasma response to shear Alfvén waves since the electrons will control the dynamics along the field due to their smaller inertia. We also assume that the cross-field drift of the electrons is negligible. Under these assumptions, we can construct a linear dispersion relation following the method of *Damiano et al.* [2003] (see Appendix A),

$$1 - \frac{2\left(\omega^2 - k_\parallel^2 v_A^2\right)}{k_\parallel^2 \theta^2 k_\perp^2 \lambda_e^2}\left[1 - \frac{1}{2\kappa} + \xi Z^*(\xi)\right] = 0, \qquad (3)$$

where ω is the wave frequency, $k_\parallel$, $k_\perp$ are the parallel and perpendicular wave numbers, respectively, $v_A = B_0(\mu_0 n_i m_i)^{-1/2}$ is the Alfvén speed, $Z^*(\xi)$ is the modified plasma dispersion function [*Summers and Thorne*, 1991], and $\xi = \omega/(k_\parallel \theta)$. Note that as $\kappa \rightarrow \infty$, this dispersion relation tends to its Maxwellian counterpart [see *Watt et al.*, 2004, equation (9)]. Note that for inertial Alfvén waves, $k_\parallel \ll k_\perp$.

[11] Figure 2 shows the solutions of the Lorentzian dispersion relation given in equation (3) (dashed and dashed-dotted lines) and the solutions of the Maxwellian dispersion relation [*Watt et al.*, 2004, equation (9)] (solid line). The plasma parameters used to obtain these solutions are $n_e = 1.5 \times 10^7$ m^{-3}, $T_e = 10$ eV, and $B_0 = 6500$ nT. The parallel wave number is kept constant at $k_\parallel = 10^{-6}$ m^{-1} and the net field-aligned drift is zero. Figure 2a shows the real frequency of the solutions, Figure 2b the damping rate, and Figure 2c the parallel phase velocity $v_{ph} = \omega/k_\parallel$ of the pulse normalized to the Alfvén speed, all as functions of the perpendicular scale length. The real solutions agree well for all values of κ (including infinity), and hence the parallel phase velocities are also in agreement ($k_\parallel$ is a constant). For a fixed value of $k_\perp$, Alfvén wave pulses should therefore propagate at the same speed along the field line, regardless of the value of κ, and will resonate with electrons travelling at those speeds. Note that $\alpha_{e,M}/v_A \sim 0.05$ for these parameters, and so the phase velocity of the inertial Alfvén waves will be much greater than $\alpha_{e,M}$ and θ_e for all values of $k_\perp$ considered here. The solutions of the linear dispersion relation for different values of $k_\parallel$ (but still assuming long parallel wavelengths) give the same phase velocities as those shown in Figure 2c and are not shown here.

[12] If we consider electron velocities greater than $\sim 2\alpha_{e,M}$, then it is clear from Figure 1 that for decreasing κ, the value of f_e at constant v increases, and so we would expect that more electrons would be available to participate in wave-particle interactions with the wave for low values of κ. This is shown quantitatively in Figure 2b, where the damping rate of the inertial Alfvén waves is greatly enhanced for low values of κ, even for small perpendicular wave number. Note that the absolute values of the damping rates will not be reproduced in simulations where the amplitude of the waves is large, since the linear approximation will no longer be valid. However, we use these solutions to the linear dispersion relation to suggest that wave-particle interactions (and hence resonant electron acceleration processes) will be stronger for low values of κ, a prediction we now test using a kinetic simulation code.

3. Kinetic Simulations

[13] We model inertial Alfvén wave (IAW) pulses using a self-consistent kinetic simulation code which has been developed to study the field-aligned electron response to shear Alfvén waves in a collisionless magnetized plasma, details of which can be found in the work of *Watt et al.* [2004]. It is assumed that the electrons carry the parallel

current associated with the pulse and that the ions carry the perpendicular current. We use the scalar potential ϕ and the parallel component of the vector potential $A_\parallel$ to describe the electromagnetic fields of the IAW pulse, where the perpendicular component of the wave magnetic field $\delta B_\perp = \nabla \times A_\parallel$, the perpendicular component of the wave electric field $\delta E_\perp = -\nabla_\perp \phi$, and the parallel component of the wave electric field $\delta E_\parallel = -\nabla_\parallel \phi - (\partial A_\parallel / \partial t)$. By using the potential description of the waves, we can describe the physical system in one dimension. The electrons are described by their distribution function $f_e(p_\parallel, z, t)$, which is allowed to evolve in time on a fixed grid in phase space according to the gyroaveraged Vlasov equation:

$$\frac{\partial f}{\partial t} + \left(p_\parallel - \frac{q_e}{m_e} A_\parallel\right) \frac{\partial f}{\partial z} + \left[\frac{q_e}{m_e}\left\{\left(p_\parallel - \frac{q_e}{m_e} A_\parallel\right) \frac{\partial A_\parallel}{\partial z} - \frac{\partial \phi}{\partial z}\right\} - \frac{\mu}{m_e} \frac{\partial B_0}{\partial z}\right] \frac{\partial f}{\partial p_\parallel} = 0, \tag{4}$$

where $p_\parallel = v_\parallel + (q_e/m_e)A_\parallel$ is the parallel canonical momentum per unit mass, $v_\parallel$ is the parallel velocity coordinate, z is the parallel spatial coordinate, and t is time. The variable change from $v_\parallel$ to $p_\parallel$ is required to avoid numerical instability in the time integration of the kinetic equation [*Jenko*, 2000].

[14] The potential variables are defined on fixed grid points in the spatial (z) domain. Using the parallel component of Ampère's Law $(\nabla \times \mathbf{B})_\parallel = \mu_0 J_\parallel$, neglecting the displacement current, and using the first moment of the distribution function as the source term for the parallel current, we obtain an expression for the parallel component of the vector potential:

$$A_\parallel = \frac{\mu_0 q_e \int_{-\infty}^{\infty} p_\parallel f dp_\parallel}{k_\perp^2 + \mu_0 \frac{q_e^2}{m_e} \int_{-\infty}^{\infty} f dp_\parallel}, \tag{5}$$

Note that the change of variables $v_\parallel \rightarrow p_\parallel$ introduces the zeroth moment of f into equation (5). We assume that all perpendicular variations can be expressed in the form $\exp(-ik_\perp x)$, where x is a perpendicular coordinate; hence the perpendicular gradients can be reduced to factors of $ik_\perp$. This assumption allows us to model the acceleration process using only one spatial dimension, thus allowing for a simulation domain of many R_E in length and high resolution in velocity space whilst retaining a reasonable run time for the simulation.

[15] The system of equations is closed by the polarization current equation, which we combine with the perpendicular component of Ampere's Law under the same assumptions as above to obtain:

$$\frac{\partial \phi}{\partial t} = -v_A^2 \frac{\partial A_\parallel}{\partial z}. \tag{6}$$

[16] In order to clearly demonstrate the effect of different distribution functions on the magnitude of the electron acceleration, we model a plasma in a uniform ambient magnetic field. A discussion of the cumulative effects of nonuniform plasma and nonuniform magnetic fields on this acceleration process is left to future publications.

[17] For the simulation results presented here, the computational domain is $L_z = 4.7R_E$ long, with $N_z = 940$ points in the z direction resulting in a uniform spatial resolution of $\Delta z = (1/200)R_E$. The point $z = 0$ represents the lower end of the simulation domain, and the z-coordinate increases with distance along the field line away from the Earth. The phase-space grid for each simulation run is determined by consideration of the amplitude of the initial pulse, the temperature of the plasma, and the functional form of the electron distribution function. Typically, there are $N_p > 240$ points in the parallel velocity direction for the electron phase-space grid. The velocity grid is unevenly spaced to allow for high resolution ($\Delta v \sim 0.1\theta_e$) of f_e for $0 < |v| < \theta_e$, but lower resolution as $|v|$ approaches the grid boundary $|v| = v_{cut}$ (typically $v_{cut} \sim v_A > 20\theta_e$).

[18] The distribution functions are initialized using the functional forms given in equation (1) and equation (2). The potentials are initially set to zero at all points in the simulation domain, and a pulse potential of the form $\phi(t) = (1/2)\phi_0(1 - \cos[2\pi(t/t_1)])$ is added to the scalar potential at the top of the simulation domain for $0 < t < t_1$, where $t_1 = 0.25$ s and ϕ_0 is the desired amplitude of the pulse. The pulse is then allowed to propagate through the simulation domain toward the lower boundary, interacting with the ambient plasma on its way. At the lower boundary, the boundary conditions for the potentials are such that the wave is partially reflected [see *Watt et al.*, 2004]: $A_\parallel = -\mu_0 \Sigma_P \phi$, where Σ_P is the height-integrated Pedersen conductivity. In this study we are interested only in the characteristics of the beam of resonant electrons formed before the pulse reaches the lower boundary.

4. Energy Flux

[19] Simulations were performed for different plasma and pulse parameters, as well as for different values of κ. In order to gain an overview of the effectiveness of the acceleration process in each case, we first define some useful variables to quantify the acceleration occurring in each simulation run. Figure 3 shows the evolution of simulation diagnostic variables at a single spatial point, $z = 1R_E$, for a typical simulation run with a Lorentzian distribution function with $\kappa = 6$. In all simulations discussed in this paper, the plasma parameters are as follows: $B_0 = 6500$ nT, $n_e = 1.5 \times 10^7$ m^{-3}, and $T_e = 10$ eV. The initial amplitude of the potential pulse is $\phi_0 = 100$ V, and the perpendicular wave number is $k_\perp \lambda_e = 2.8$, yielding an initial perpendicular electric field of $E_\perp = 200$ mV/m. Figure 3a shows a contour plot of the distribution function $f_e(v_\parallel)$ as a function of time, while Figure 3b shows the absolute value of the energy flux $Q_\parallel(t) = \int_{-\infty}^{\infty} v_\parallel^3 f_e(v_\parallel, t)\, dv_\parallel$ at the same location (the absolute value is taken since the downward direction is negative, and the pulse accelerates the electrons in the negative $v_\parallel$ direction). Before the electromagnetic SAW pulse reaches the location $z = 1R_E$ at $t = 1.72$ s, a distinct beam is seen at large negative velocities. The ambient distribution function remains stationary, however, until the pulse arrives. The enhancement in $Q_\parallel$ for $t < 1.72$ s is therefore solely due to the beam, since a stationary distribution function will yield zero energy flux. We choose the energy flux as a means to quantify the acceleration process, as well as considering the velocity/energy ranges of the accelerated particles (see section 5).

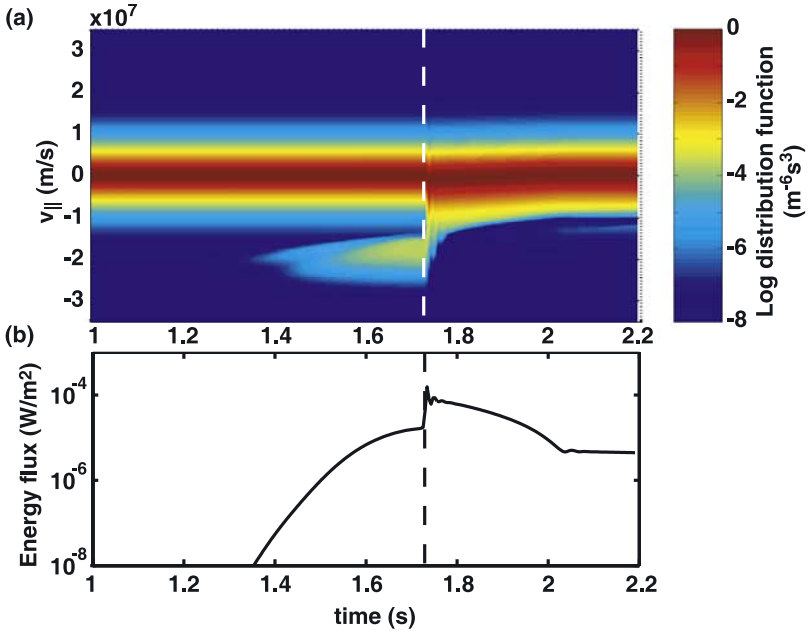

Figure 3. (a) Evolution of one-dimensional distribution function at $z = 1R_E$ for pulse amplitude of $\phi_0 = 100$ V and $k_\perp \lambda_e = 2.8$. (b) Evolution of absolute electron energy flux at the same location for the same simulation run (absolute value taken since electron acceleration by the pulse is in downward (negative) direction). Pulse arrives at $z = 1R_E$ at $t = 1.72$ s.

[20] We now focus on how the energy flux of the accelerated beam changes when the κ parameter is changed. Figure 4 shows the energy flux $Q_\parallel$ as a function of time at $z = 1R_E$ from seven different simulations, one initialized with a Maxwellian plasma (black line), the others initialized with Lorentzian functions with different values of κ (colored lines). In each simulation run, the initial pulse potential is $\phi_0 = 67$ V and the perpendicular wavelength is $k_\perp \lambda_e = 2.1$ (corresponding to $E_\perp = 100$ mV/m). For all simulation runs shown in this figure, the pulse arrives at $z = 1R_E$ at $t = 1.45$ s. In every simulation with a Lorentzian distribution function, we see an enhancement of $Q_\parallel$ prior to the pulse arrival, which is evidence of energetic beam formation due to the resonant acceleration process. However, in the Maxwellian case, no such beam is apparent. The amount of energy flux in the beam increases rapidly as κ is decreased, demonstrating that, as predicted, the amount of electron acceleration is increased dramatically for distribution functions with a high-energy tail.

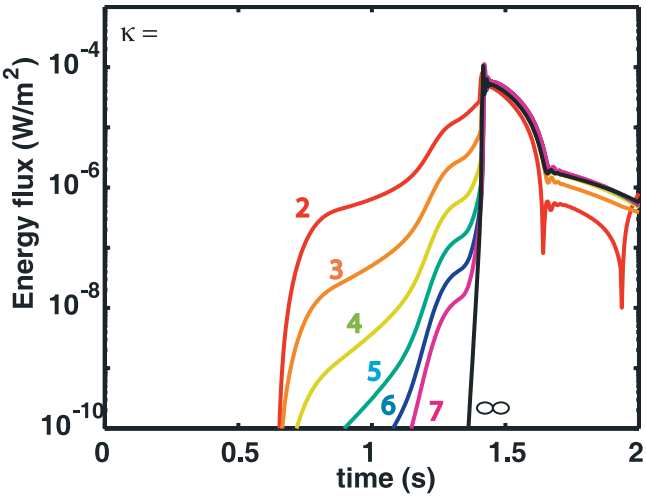

Figure 4. Evolution of absolute electron energy flux at $z = 1R_E$ for seven different simulation runs with same plasma parameters but different values of κ. All simulations studied an initial pulse with $\phi_0 = 67$ V and $k_\perp \lambda_e = 2.1$. Colored lines show results from simulations with Lorentzian distribution functions, black line shows results from Maxwellian simulation.

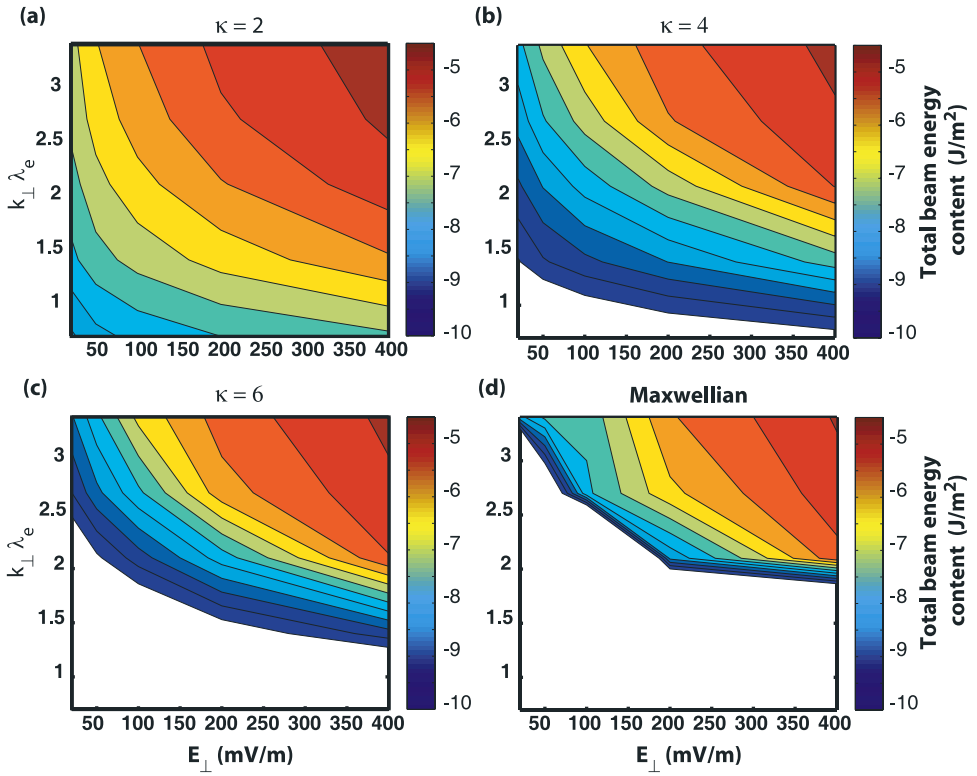

Figure 5. Contour plots showing the variation of total beam energy content (K_{beam}) with amplitude and perpendicular scale length of the pulse for (a) $\kappa = 2$, (b) $\kappa = 4$, (c) $\kappa = 6$, and (d) Maxwellian distribution function. White areas show pulse parameters for which no significant resonantly accelerated electron beam is formed.

[21] A good indicator of the total amount of beam energy is the integral of energy flux $K_{beam} = \int_0^{t_p} Q_{\parallel} dt$ at $z = 1R_E$, where t_p is the time at which the pulse reaches the location $z = 1R_E$, e.g., the dashed vertical line in Figure 3. We have evaluated K_{beam} (measured in J/m^2) for 100 simulation runs with varying initial pulse amplitude and perpendicular scale length in order to explore the pulse parameter space. The results are summarized in Figure 5, which shows contour plots of K_{beam} as a function of $k_\perp \lambda_e$ and initial $E_\perp$ for four different values of κ: $\kappa = 2$ (Figure 5a), $\kappa = 4$ (Figure 5b), $\kappa = 6$ (Figure 5c), and $\kappa = \infty$ (Maxwellian) (Figure 5d). Twenty-five simulations were performed for each value of κ with the following sets of pulse variables: initial $E_\perp = 20$, 50, 100, 200, 400 mV/m and $k_\perp \lambda_e = 0.7$, 1.4, 2.1, 2.8, 3.4. The white regions indicate those amplitudes and perpendicular scale lengths for which no significant energized electron beam was formed due to wave-particle interactions. Figure 5 clearly shows that the electron acceleration process becomes much more efficient for low values of κ. For $\kappa = 2$, there is always beam formation in the simulation, even for low amplitudes and $k_\perp \lambda_e < 1$. The values of K_{beam} are also highest for $\kappa = 2$. As κ becomes larger, there are some values of $k_\perp \lambda_e$ for which no significant beam is generated, regardless of the amplitude of the pulse. For example, with $\kappa = 4$, there is no beam generation for $k_\perp \lambda_e \leq 0.7$, while for $\kappa = 6$ there is no beam generation for $k_\perp \lambda_e \leq 1.4$. For the Maxwellian distribution function, beams do not form for $k_\perp \lambda_e < 2.1$. In the Maxwellian simulation set, it is only for the very short perpendicular scale lengths ($k_\perp \lambda_e \geq 3.4$) that any significant beam is formed for small pulse amplitudes ($E_\perp \leq 50$ mV/m). For small κ, the amount of energy in the beam gradually increases as one moves from the bottom left (low pulse amplitude, larger perpendicular scale length) to the top right (high pulse amplitude, small perpendicular scale length) of Figures 5a and 5b. This is not the case for Maxwellian distributions, where there is a strong gradient in K_{beam} for high amplitudes as the perpendicular scale length is decreased (i.e., moving from bottom right to top right of Figure 5d). This suggests that the strong threshold conditions discovered using Maxwellian distribution functions [*Watt et al.*, 2005] may be relaxed for more realistic Lorentzian distribution functions.

5. Energy Range

[22] Although it is instructive to know which pulse and plasma parameters affect the amount of energy in resonant beam electrons, it is also useful to know the energy range of the accelerated electrons. We can determine the velocity (energy) range of an electron beam by studying the electron distribution function at a fixed spatial position $z = 1R_E$, for all times before the arrival of the pulse. We are only concerned here with those simulations which provide enough total beam energy to register in the scale defined by Figure 5. As can be seen in Figure 3a, the velocity range of beam electrons is well-defined, and the beam component f_b falls off steeply with v at the beam edges.

[23] We compare the highest and lowest velocities of accelerated electrons in Figure 6, showing different perpendicular scale lengths, $k_\perp \lambda_e = 0.7$ (Figure 6a), 1.4 (Figure 6b), 2.1 (Figure 6c), 2.8 (Figure 6d), and 3.4 (Figure 6e). In each case the lowest energy electrons in the beam travel with the pulse phase velocity. The resonant acceleration process by inertial Alfvén waves in a uniform plasma is essentially one-interaction Fermi acceleration [*Kletzing*, 1994], and so the lowest velocity expected from this process is just larger than the phase speed of the pulse. The lowest electron beam velocity observed in any of the simulations is therefore determined only by the perpendicular scale length and is unaffected by initial pulse amplitude or by the form of the distribution function. We indicate the lowest beam electron velocity by a solid black circle in each figure. As the perpendicular scale length is decreased (moving from Figure 6a through to Figure 6e), the lowest beam energy decreases, following the phase velocity of the pulse, which decreases as $k_\perp \lambda_e$ is increased.

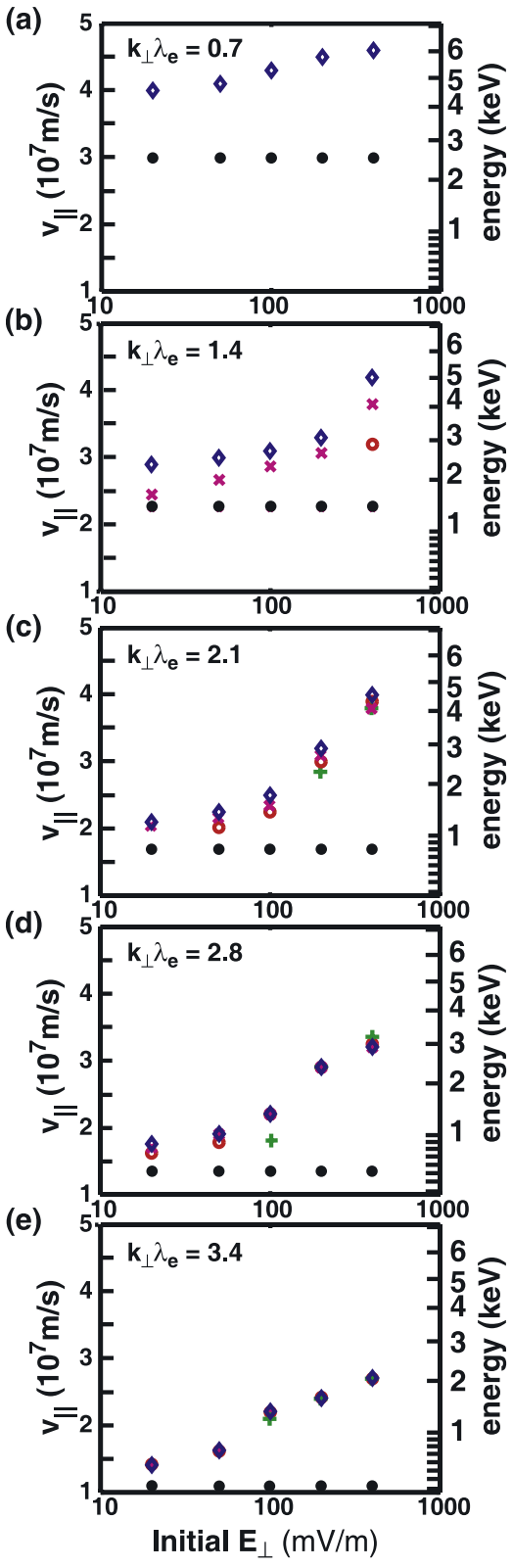

[24] The highest energy of the beam electrons is dependent upon the initial pulse amplitude and on the form of the distribution function. To illustrate this, different symbols are used in Figure 6 to distinguish the upper velocity limit of the resonant beam electrons observed for different forms of the electron distribution function: $\kappa = 2$ (blue diamonds), $\kappa = 4$ (magenta crosses), $\kappa = 6$ (red circles), and Maxwellian distribution function (green pluses). Note that for the lowest values of $k_\perp \lambda_e$, only simulations with low values of κ are shown because significant electron beams are not generated for high values of κ and low values of $k_\perp \lambda_e$ (see previous section). Once the minimum conditions for electron beam formation are satisfied (see Figure 5), then the upper velocity range of the accelerated electrons increases with increasing pulse amplitude for all perpendicular scale lengths and all values of κ. Again, this is consistent with one-interaction Fermi acceleration. In most cases, the upper velocity range of beam electrons does not depend upon the form of the distribution function. However, where there are differences between simulations with the same pulse parameters but different electron distribution functions, then the lowest values of κ always provide the highest beam velocities. This is particularly clear for high initial pulse amplitudes. For example, in Figure 6(b), $\kappa = 6$ (red circle) gives a lower value than $\kappa = 4$ (magenta cross), which in turn is lower than $\kappa = 2$ (blue diamond). The differences are mainly confined to $k_\perp \lambda_e = 0.7, 1.4$. For these perpendicular scale lengths, the acceleration process is not very efficient for large values of κ (see Figure 5), and this may explain why the maximum velocity of the accelerated beam electrons is smaller.

6. Wave Poynting Flux Conversion

[25] One of the advantages to using a self-consistent computer model is that we can quantitatively study the conversion

Figure 6. Velocity ranges of resonantly accelerated electron beams for each value of pulse amplitude and perpendicular scale length studied. Solid black circles indicate the lowest observed electron beam velocity for each parameter set (does not depend upon initial pulse amplitude or form of the distribution function). The maximum velocity of the beam electrons is shown by color-coded symbols: blue diamonds indicate simulations with $\kappa = 2$, magenta crosses indicate $\kappa = 4$, red circles indicate $\kappa = 6$, and green pluses indicate Maxwellian distribution functions. Velocity ranges are shown as a function of pulse amplitude for $k_\perp \lambda_e$ = (a) 0.7, (b) 1.4, (c) 2.1, (d) 2.8, and (e) 3.4.

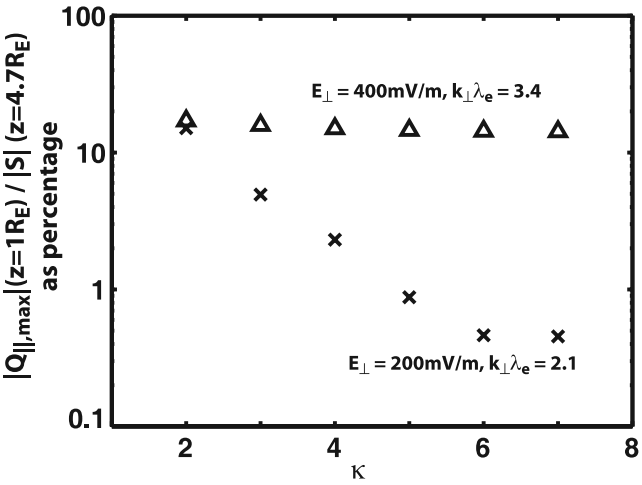

Figure 7. Ratio of parallel electron energy flux at $z = 1R_E$ to magnitude of the Poynting vector at $z = 4.7R_E$ as a function of κ for $E_\perp = 400$ mV/m, $k_\perp\lambda_e = 3.4$ (triangles) and $E_\perp = 200$ mV/m, $k_\perp\lambda_e = 2.1$ (crosses).

of wave energy to particle energy as a result of the inertial Alfvén wave interaction with the electrons. We compute the maximum electron energy flux due to the resonantly accelerated electron beam $|Q_\parallel,\max|$ at $z = 1R_E$ and compare it with the magnitude of the wave Poynting vector $|\mathbf{S}|$ as the wave enters the simulation domain at $z = 4.7R_E$. This ratio can then be used as a measure of the efficiency of the wave-particle interaction process.

[26] Figure 7 shows the percentage ratio $|Q_\parallel,\max|/|\mathbf{S}|$ as a function of κ for two different sets of wave parameters. Case 1 has $E_\perp = 400$ mV/m and $k_\perp\lambda_e = 3.4$ (denoted by triangles) and case 2 has $E_\perp = 200$ mV/m and $k_\perp\lambda_e = 2.1$ (denoted by crosses). Although these wave parameters are at the more extreme end of the parameter study, each case provides data for a number of different values of κ and so trends can be established. For case 1 (triangles), the percentage conversion of wave energy to particle energy is around 15–17% and does not vary with κ. On the other hand, case 2 (crosses) shows a strong dependence on κ. The percentage conversion of wave energy to particle energy is roughly the same as in case 1 for $\kappa = 2$ but drops off sharply as κ is increased and is only a fraction of 1% for $\kappa = 6, 7$.

[27] For case 1 the phase velocity of the waves will be reduced to $\sim 0.3v_A$ and the distribution function will be strongly perturbed by the large amplitude wave. The existence of a high-energy tail in the distribution function therefore makes little difference to the efficiency of the wave-particle interaction because the large-amplitude wave shifts all the distribution functions in $v_\parallel$ such that a significant number of electrons in each distribution function are able to take part in the acceleration process. However, if we consider case 2, where the phase velocity of the waves is higher ($\sim 0.4v_A$) and the wave amplitude is halved, then the distribution function is less perturbed in the wave field. Under these circumstances, the high-energy tail of the low κ distribution functions becomes important for the efficiency of the wave-particle interaction. Without the high-energy tail, i.e., for high values of κ, there are insufficient electrons with $v_\parallel = v_{ph}$ to take energy from the wave, and the efficiency of the wave acceleration process is low (<1%).

[28] The percentage conversion of wave energy to particle energy also depends upon the original amplitude of the wave. Figure 8 shows the same ratio $|Q_\parallel,\max|/|\mathbf{S}|$ as a function of $|\mathbf{S}|$ for simulations with different values of κ (indicated using the same colored symbols as in section 5). Results for two values of perpendicular scale length are shown $k_\perp\lambda_e = 2.1$ (Figure 8b) and $k_\perp\lambda_e = 3.4$ (Figure 8b). In Figure 8a the percentage conversion of wave energy to particle energy for $\kappa \geq 4$ is very small (<1%) for small-amplitude waves but rises sharply as the wave amplitude increases to ~10% for the highest-amplitude waves studied in this paper ($E_\perp = 400$ mV/m). In contrast, when $\kappa = 2$, the percentage conversion of particle energy to wave energy is high for small-amplitude waves (~30%) and decreases as the wave amplitude is increased. This indicates that for $\kappa = 2$, there are always electrons with $v_\parallel = v_{ph}$ ready to take part in resonant interaction with the wave, whereas for higher values of κ, there are only significant numbers of electrons with $v_\parallel = v_{ph}$ once the distribution function has been moved in $v_\parallel$-space by a large-amplitude wave.

[29] This trend is continued at even shorter perpendicular wavelengths, as seen in Figure 8b. In this case, for $\kappa = 2$ and small wave amplitudes, almost all the wave poynting flux has been converted to electron energy flux by the time the

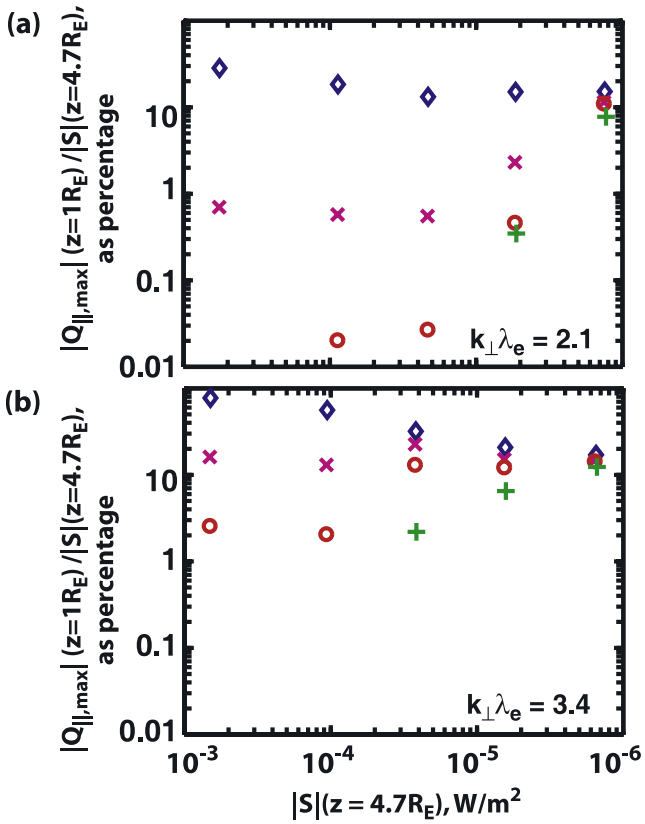

Figure 8. Ratio of parallel electron energy flux at $z = 1R_E$ to magnitude of the Poynting vector at $z = 4.7R_E$ for increasing wave amplitude and for (a) $k_\perp\lambda_e = 2.1$, and (b) $k_\perp\lambda_e = 3.4$. Color-coded symbols denote different values of κ: blue diamonds show $\kappa = 2$, magnenta crosses show $\kappa = 4$, red circles show $\kappa = 6$, and green pluses show simulations with Maxwellian distribution functions.

wave has travelled a distance of $3.7R_E$ along the field line. However, the conversion of wave energy to electron energy is similar ($\sim$10%) for the high-amplitude waves as it is in Figure 8a, suggesting that for large amplitude waves there is an upper limit to the fraction of energy which may be extracted from the wave by the inertial Alfvén wave energization process.

7. Discussion

[30] Previous studies [*Watt et al.*, 2005] of electron acceleration due to inertial Alfvén waves have revealed that this process can only occur within a rather restricted range of wave and plasma parameters. *Watt et al.* [2005] found that thresholds in both pulse amplitude and perpendicular scale length must be exceeded before a particular inertial Alfvén wave pulse will accelerate enough electrons to form a significant beam. For plasma parameters indicative of conditions at 7000 km in the auroral zone, it was found that only pulses with $k_\perp \lambda_e \geq 2.7$ or amplitudes of $\phi_0 \geq 50$ V could generate resonant electron beams in a uniform plasma. It is obvious from Figure 5 that this is not the case in the presence of more realistic distribution functions. In particular, a high-energy tail in the distribution function allows the resonant acceleration process to operate where it would otherwise be shut off for a Maxwellian distribution function. Resonant electron acceleration can therefore occur in Lorentzian plasmas for larger perpendicular scale lengths than can generate resonantly accelerated electrons in a Maxwellian plasma.

[31] It is not simply a question of whether a beam may be formed. If the accelerated electrons are to contribute toward auroral brightening, then we must also determine the energies of the beam electrons. When Lorentzian distribution functions are considered, it is possible to accelerate electrons to much higher energies than previously expected, using relatively low-amplitude waves, although there are stringent conditions on this process: the perpendicular scale length of the pulse should not be too small or else the phase velocity will be reduced so much that the accelerated electrons have energies of only $\sim$100 s of eV. However, if the phase velocity remains a large fraction of the Alfvén speed, then a low value of κ is required, in order to provide sufficient electrons with $v \sim v_{ph}$ for the resonant acceleration process. If these conditions are satisfied, then keV electrons can easily be attained, even for relatively small-amplitude waves (see Figure 6a).

[32] A limitation of our results is that we have performed these simulations for uniform plasma conditions and a uniform magnetic field. Kinetic simulations incorporating a nonuniform magnetic field and hence including the effects of an increasing Alfvén velocity gradient and mirror effects have recently been performed by *Watt et al.* [2006]. They show that as the pulse travels down toward the ionosphere through an increasing magnetic field gradient, the phase velocity of the pulse increases. The pulse can therefore catch up with electrons that have already been accelerated by the pulse parallel electric field to accelerate them to even higher energies. The energy ranges depicted in Figure 6 are therefore underestimates, since the lowest energy of beam electrons reaching the upper ionosphere will likely be equal to the peak pulse phase velocity along the field line. The highest energy of electrons in the beam may also be increased when a nonuniform magnetic field is included in the simulation because the electrons may undergo repeated acceleration by the pulse. Also, the fraction of Poynting flux which is converted to electron energy flux may also be increased if the wave has a chance to accelerate the electrons at more than one location. It is quite possible that the percentage ratios shown in Figures 7 and 8 are underestimates.

[33] Self-consistent simulations which study the effects of nonuniform density and temperature profiles along the field line, as well as including a static potential drop in addition to the Alfvén wave acceleration mechanism have yet to be attempted. It is clear that factors which increase the number of electrons with $v \sim v_{ph}$ as the pulse moves through the plasma will increase the effectiveness of inertial Alfvén wave acceleration (e.g., decreasing the pulse v_{ph}, increasing the pulse amplitude, or as we have seen in this study, changing the form of the electron distribution function). On the other hand, factors which decrease the phase space density of electrons at $v \sim v_{ph}$ will decrease the effectiveness. It may be that including a realistic temperature profile, for example, will help to impose a stricter altitude range for the acceleration mechanism, since cold electrons at the ionospheric end of the field line, regardless of their functional form in phase space, will not be resonant with the wave unless the wave amplitude is very large.

8. Conclusions

[34] We have investigated the characteristics of electron acceleration by inertial Alfvén waves. Informed by in situ observations, we study Lorentzian (kappa) distribution functions using a new form of the kinetic dispersion relation and a self-consistent kinetic simulation code. The kinetic dispersion relation suggests that the frequency and parallel phase velocity of the waves does not change with the form of the electron distribution function but that the damping rate is increased significantly for low values of $\kappa \leq 7$. From these solutions it is therefore expected that wave-particle interactions between inertial Alfvén waves and electrons will be enhanced for distribution functions with a high-energy tail (i.e., low κ).

[35] The predictions suggested by the solutions of the linear dispersion relation have been tested with a self-consistent nonlinear simulation code. The simulation results show that the efficiency of the electron acceleration process is indeed greatly enhanced in the presence of Lorentzian distribution functions, with the lowest values of κ corresponding to the most energetic electron beams, for all pulse amplitudes and perpendicular scale lengths studied in this paper. The lowest energy of the beam electrons is determined by the phase speed of the wave as it travels through the plasma [c.f. *Kletzing*, 1994; *Watt et al.*, 2005]. The highest energy of the beam electrons increases with increasing amplitude of the pulse, but is also affected by the value of κ. Most importantly, those pulses with amplitudes and perpendicular scales which would not resonantly accelerate electrons in a Maxwellian plasma are shown to generate significant beams in realistic plasmas with Lorentzian distribution functions. The percentage efficiency of converting wave Poynting flux to electron energy flux is shown to have a complicated relationship

with wave amplitude, perpendicular scale length, and the value of κ, although generally speaking, the smaller the value of κ, the more energy can be extracted from the wave through the resonant electron interaction. The stringent conditions determined by *Watt et al.* [2005] for resonant electron acceleration due to inertial Alfvén waves in Maxwellian plasmas may therefore be relaxed for more realistic plasma distribution functions.

Appendix A: Derivation of Inertial Alfvén Wave Dispersion Relation

[36] We follow a similar analysis to *Damiano et al.* [2003], beginning with the cold plasma dispersion relation:

$$\omega^2 = k_{||}^2 v_A^2 \left(1 + \frac{ik_{||}^2}{\omega\mu_0\sigma_{||}}\right)^{-1}, \tag{A1}$$

where an Ohm's Law $\sigma_{||} = j_{||}/E_{||}$ is used to relate the field-aligned conductivity to the field aligned current and electric field. In order to include the kinetic effects of the Lorentzian distribution function, we need to calculate the parallel current $j_{||}$ generated by perturbations in the electron distribution function f_1. We assume that the ions do not contribute to the parallel current and write

$$j_{||} = q_e \int_{-\infty}^{\infty} v_{||} f_1 dv_{||} \tag{A2}$$

If we neglect the perpendicular electron drift (assuming the $\mathbf{E} \times \mathbf{B}$ drift is negligible, and ignoring polarization and curvature drifts), then we can linearize the appropriate Vlasov equation and express the distribution function perturbation as

$$f_1 = \frac{1}{(k_{||}v_{||} - \omega)}\left[i\frac{q_e}{m_e}E_{||}\frac{\partial f_0}{\partial v_{||}}\right] \tag{A3}$$

where we assume there is no equilibrium $E_{||}$, and $f_1 \ll f_0$.

[37] We use a one-dimensional Lorentzian distribution function for the equilibrium electron distribution function f_0 (equation (1)) and substitute its derivative into equation (A3) so that we can express the parallel current as

$$j_{||} = -2i\frac{nq_e^2}{m_e}\frac{E_{||}}{\sqrt{\pi}\theta^3}\left(\frac{\Gamma(\kappa+1)}{\kappa^{3/2}\Gamma(\kappa-1/2)}\right)\int_{-\infty}^{\infty}\frac{v_{||}^2}{k_{||}v_{||}-\omega} \cdot \left(1 + \frac{v_{||}^2}{\kappa\theta^2}\right)^{-(\kappa+1)} dv_{||} \tag{A4}$$

Perform a change of variables such that $h = v_{||}/\theta$:

$$j_{||} = -\frac{2i\omega_{pe}^2\epsilon_0}{k_{||}\theta}\frac{1}{\sqrt{\pi}}E_1\left(\frac{\Gamma(\kappa+1)}{\kappa^{\frac{3}{2}}\Gamma\left(\kappa-\frac{1}{2}\right)}\right)\int_{-\infty}^{\infty}\frac{h^2}{h-\xi} \cdot \left(1+\frac{h^2}{\kappa}\right)^{-(\kappa+1)} dh. \tag{A5}$$

where $\xi = \omega/(k_{||}\theta)$. Let us rewrite the integral with respect to h in the above expression (hereinafter denoted as I) in the following form:

$$I = \int_{-\infty}^{\infty}(h+\xi)\left(1+\frac{h^2}{\kappa}\right)^{-(\kappa+1)} dh + \xi^2\int_{-\infty}^{\infty}\frac{1}{h-\xi}\left(1+\frac{h^2}{\kappa}\right)^{-(\kappa+1)} dh. \tag{A6}$$

Note that the modified plasma dispersion function $Z^*(\xi)$ is given by [*Summers and Thorne*, 1991]:

$$Z^*(\xi) = \frac{1}{\sqrt{\pi}}\frac{\Gamma(\kappa+1)}{\kappa^{\frac{3}{2}}\Gamma\left(\kappa-\frac{1}{2}\right)}\int_{-\infty}^{\infty}\frac{ds}{(s-\xi)(1+(s^2/\kappa))^{\kappa+1}} \tag{A7}$$

and so the necessary integral for the modified plasma dispersion function can be identified in the second term in equation (A6). Thus we focus on the first term on the right hand side, which can be written:

$$I_{(1)} = \kappa^{\kappa+1}\int_{-\infty}^{\infty} h\left(\kappa+h^2\right)^{-(\kappa+1)} dh + \xi\kappa^{\kappa+1}\int_{-\infty}^{\infty}\left(\kappa+h^2\right)^{-(\kappa+1)} dh. \tag{A8}$$

The first term on the right-hand side of equation (A8) can be shown to be zero (e.g., one can perform another change of variables $u = h^2$). The second term in equation (A8) is an improper integral of a common form and has a general solution [*Gradshteyn and Ryzhik*, 2000]:

$$\int_{-\infty}^{\infty}\frac{dx}{(ax^2+2bx+c)^n} = \frac{(2n-3)!!\pi a^{n-1}}{(2n-2)!!(ac-b^2)^{n-1/2}} \tag{A9}$$

where, in our case, $n = \kappa + 1$, $a = 1$, $b = 0$, and $c = \kappa$ (remembering that κ is always an integer); hence equation (A8) becomes

$$I_{(1)} = \xi\kappa^{1/2}\frac{(2\kappa-1)!!\pi}{(2\kappa)!!} \tag{A10}$$

Returning to equation (A5) and performing appropriate substitutions for the integral, we have

$$j_{||} = -\frac{2i\omega_{pe}^2\epsilon_0}{k_{||}\theta}E_1\left[\xi\left(1-\frac{1}{2\kappa}\right)+\xi^2 Z^*(\xi)\right]. \tag{A11}$$

This expression for $j_{||}$ can now be used to obtain $\sigma_{||}$ for equation (A1), which is then rearranged into a more familiar form

$$1 - \frac{2\left(\omega^2 - k_{||}^2 v_A^2\right)}{k_{||}^2\theta^2 k_\perp^2\lambda_e^2}\left[1-\frac{1}{2\kappa}+\xi Z^*(\xi)\right] = 0. \tag{A12}$$

Note that as $\kappa \to \infty$, this dispersion relation tends to its Maxwellian counterpart [see *Watt et al.*, 2004], remembering that $Z'(\xi) = -2(1 + \xi Z(\xi))$ [*Fried and Conte*, 1961].

[38] **Acknowledgments.** CEJW is funded by the Canadian Space Agency and NSERC. This work has in part been enabled by the use of Westgrid computing resources, which are funded in part by the Canada Foundation for Innovation, Alberta Innovation and Science, BC Advanced Education, and the participating research institutions.

[39] Zuyin Pu thanks G. Lakhina and another reviewer for their assistance in evaluating this paper.

References

Abramowitz, M., and I. A. Stegun (1972), *Handbook of Mathematical Functions with Formulas, Graphs, and Mathematical Tables*, 9th Ed., pp. 255–258, Dover, New York.

Andersson, L., N. Ivchenko, J. H. Clemmons, A. A. Namgaladze, B. Gustavsson, J.-E. Wahlund, L. Eliasson, and R. Y. Yurik (2002), Electron signatures and Alfvén waves, *J. Geophys. Res.*, *107*(A9), 1244, doi:10.1029/2001JA900096.

Boehm, M. H., C. W. Carlson, J. P. McFadden, and F. S. Mozer (1990), High-resolution sounding rocket observations of large-amplitude Alfvén waves, *J. Geophys. Res.*, *95*, 12,157.

Chaston, C. C., C. W. Carlson, R. E. Ergun, and J. P. McFadden (2000), Alfvén waves, density cavities and electron acceleration observed from the FAST spacecraft, *Phys. Scr. T*, *84*, 64.

Chaston, C. C., J. W. Bonnell, L. M. Peticolas, C. W. Carlson, and J. P. McFadden (2002), Driven Alfvén waves and electron acceleration: A FAST case study, *Geophys. Res. Lett.*, *29*(11), 1535, doi:10.1029/2001GL013842.

Chaston, C. C., J. W. Bonnell, C. W. Carlson, J. P. McFadden, R. E. Ergun, and R. J. Strangeway (2003), Properties of small-scale Alfvén waves and accelerated electrons from FAST, *J. Geophys. Res.*, *108*(A4), 8003, doi:10.1029/2002JA009420.

Chaston, C. C., et al. (2005), Energy deposition by Alfvén waves into the dayside auroral oval: Cluster and FAST observations, *J. Geophys. Res.*, *110*, A02211, doi:10.1029/2004JA010483.

Chen, L.-J., C. A. Kletzing, S. Hu, and S. R. Bounds (2005), Auroral electron dispersion below inverted-V energies: Resonant deceleration and acceleration by Alfvén waves, *J. Geophys. Res.*, *110*, A10S13, doi:10.1029/2005JA011168.

Christon, S. P., D. G. Mitchell, D. J. Williams, L. A. Frank, C. Y. Huang, and T. E. Eastman (1988), Energy spectra of plasma sheet ions and electrons from ~50 eV/e to ~1 MeV during plasma temperature transitions, *J. Geophys. Res.*, *93*, 2562.

Clark, A. E., and C. E. Seyler (1999), Electron beam formation by small-scale oblique inertial Alfvén waves, *J. Geophys. Res.*, *104*, 17,233.

Damiano, P. A., R. D. Sydora, and J. C. Samson (2003), Hybrid Magnetohydrodynamic-kinetic model of standing shear Alfvén waves, *J. Plasma Phys.*, *69*, 277.

Ergun, R. E., L. Andersson, Y.-J. Su, D. L. Newman, M. V. Goldman, W. Lotko, C. C. Chaston, and C. W. Carlson (2005), Localized parallel electric fields associated with inertial Alfvén waves, *Phys. Plasmas*, *12*, 072901, doi:10.1063/1.1924495.

Fried, B. D., and S. D. Conte (1961), *The Plasma Dispersion Function*, Elsevier, New York.

Goertz, C. K., and R. W. Boswell (1979), Magnetosphere-ionosphere coupling, *J. Geophys. Res.*, *84*, 7239.

Gradshteyn, I. S., and I. M. Ryzhik (2000), *Table of Integrals, Series and Products*, 6th Ed., p. 322, Elsevier, New York.

Hasegawa, A. (1976), Particle acceleration by MHD surface-wave and formation of aurora, *J. Geophys. Res.*, *81*, 5083.

Hui, C. H., and C. E. Seyler (1992), Electron acceleration by Alfvén waves in the magnetosphere, *J. Geophys. Res.*, *97*, 3953.

Ivchenko, N., G. Marklund, K. Lynch, D. Pietrowski, R. Torbert, F. Primdahl, and A. Ranta (1999), Quasiperiodic oscillations observed at the edge of an auroral arc by Auroral Turbulence 2, *Geophys. Res. Lett.*, *26*, 3365.

Jenko, F. (2000), Massively parallel Vlasov simulation of electromagnetic drift-wave turbulence, *Comp. Phys. Comm.*, *125*, 196.

Khoyaintsev, Y., N. Ivchenko, K. Stasiewicz, and M. Berthomier (2000), Electron energization by Alfvén waves: Freja and sounding rocket observations, *Phys. Scr. T*, *84*, 151.

Kletzing, C. A. (1994), Electron acceleration by Kinetic Alfvén waves, *J. Geophys. Res.*, *99*, 11,095.

Kletzing, C. A., J. D. Scudder, E. E. Dors, and C. Curto (2003), Auroral source region: Plasma properties of the high-latitude plasma sheet, *J. Geophys. Res.*, *108*(A10), 1360, doi:10.1029/2002JA009678.

Lysak, R. L., and C. W. Carlson (1981), The effect of microscopic turbulence on magnetosphere-ionosphere coupling, *Geophys. Res. Lett.*, *8*, 269.

Lysak, R. L., and W. Lotko (1996), On the kinetic dispersion relation for shear Alfvén waves, *J. Geophys. Res.*, *101*, 5085.

Olsson, A., and P. Janhunen (1998), Field-aligned conductance values estimated from Maxwellian and kappa distributions in quiet and disturbed events using Freja electron data, *Ann. Geophys.*, *16*, 298.

Seyler, C. E., J.-E. Wahlund, and B. Holback (1995), Theory and simulation of low-frequency plasma waves and comparison to Freja satellite observations, *J. Geophys. Res.*, *100*, 21,453.

Su, Y.-J., S. T. Jones, R. E. Ergun, and S. E. Parker (2004), Modeling of field-aligned electron bursts by dispersive Alfvén waves in the dayside auroral region, *J. Geophys. Res.*, *109*, A11201, doi:10.1029/2003JA010344.

Summers, D., and R. M. Thorne (1991), The modified plasma dispersion function, *Phys. Fuilds*, *3*, 1835.

Thompson, B. J., and R. L. Lysak (1996), Electron acceleration by inertial Alfvén waves, *J. Geophys. Res.*, *101*, 5359.

Watt, C. E. J., and R. Rankin (2007), Parallel electric fields associated with inertial Alfvén waves, *Planet. Space Sci.*, in press.

Watt, C. E. J., R. Rankin, and R. Marchand (2004), Kinetic simulations of electron response to shear Alfvén waves in magnetospheric plasmas, *Phys. Plasmas*, *11*, 1277.

Watt, C. E. J., R. Rankin, I. J. Rae, and D. M. Wright (2005), Self-consistent electron acceleration due to inertial Alfvén wave pulses, *J. Geophys. Res.*, *110*, A10S07, doi:10.1029/2004JA010877.

Watt, C. E. J., R. Rankin, I. J. Rae, and D. M. Wright (2006), Inertial Alfvén waves and acceleration of electrons in non-uniform magnetic fields, *Geophys. Res. Lett.*, *33*, L02106, doi:10.1029/2005GL024779.

R. Rankin and C. E. J. Watt, Department of Physics, University of Alberta, Edmonton, AB T6G 0T1 Canada.